Cyclotron Resonance in Germanium*

RALPH R. GOODMAN†
Department of Physics, University of Michigan, Ann Arbor, Michigan
(Received April 25, 1960; revised manuscript received January 9, 1961)

Early cyclotron resonance for holes in Ge gave evidence of two resonant peaks associated with the so-called light and heavy holes. Luttinger and Kohn predicted, on the basis of a careful investigation of the theory of degenerate bands, that at low enough temperatures additional peaks should appear. Subsequent experiments confirmed this prediction. In this paper a comparison is made of the cyclotron resonance theory and the experiments of Fletcher, Yaeger, and Merritt. Values of the effective mass constants which best fit the data are found. Resonant peaks additional to those found by Fletcher, Yaeger, and Merritt are predicted and discussed.

I. INTRODUCTION

ONE of the principal methods of describing the motion of charge carriers in perturbed periodic fields is the so-called effective-mass theory. In this method the effect of the periodic potential on the motion of a charge is replaced, under certain conditions, by terms which appear in the equations of motion much in the same way that the mass appears in the free-electron case. In the simplest band theory these constants take on the form of a tensor.[1] Several authors[2] have extended the theory to include degenerate bands and found that the effective-mass constants enter in a more complicated form. It is well known that degenerate band theory is required in order to describe the valence band for both silicon and germanium.[3] Luttinger[4] has given the most general form of the Hamiltonian for such cases and has shown that in the presence of an external magnetic field five constants are needed for the valence band in both silicon and germanium.

One method of finding the effective-mass constants is by cyclotron resonance absorption methods.[5] Values for the effective-mass constants have been reported by several writers.[2] In these experiments, however, only two resonant peaks appeared for both germanium and silicon. Luttinger and Kohn[6] found that more peaks were predicted at lower temperatures since the spacing of the energy levels becomes nonuniform at low quantum numbers. The experiments of Fletcher, Yaeger, and Merritt[7] showed this to be the case for germanium. Their experiments gave many resonant peaks at the lowest temperature considered (1.3°K). These peaks gave way to only two prominent peaks as the temperature was raised to 4.2°K.

It is the purpose of this paper to fit the theory of JML and LK to the experimental results of FYM in order to determine the best values of the effective-mass constants. In Sec. II it is shown that for a "germanium-like" crystal the momentum along the direction of the magnetic field may be taken to be zero without introducing appreciable error. The determination of the effective-mass constants is given in Sec. III.

For the details of the development of the theory of cyclotron resonance in degenerate bands, the reader is referred to JML. Deviations from the equations in JML are mentioned as they appear.

II. A TEST OF THE $P_H=0$ ASSUMPTION

Solutions to the general equation

$$D\psi=E\psi, \tag{1}$$

where D is given by Eq. (45) in JML, are, in general, not known. There are, however, two special cases which may be solved. These are (1) if the momentum component along the magnetic field direction (P_H) is zero and (2) if the effective mass constants γ_2 and γ_3 given by JML are equal. In an earlier paper[8] it was shown that the assumption is valid in the classical limit and leads to errors of less than 3% in the cyclotron resonance absorption peaks. It will now be shown that it is also valid in the quantum limit for germanium.

The rough estimate of γ_2 and γ_3 obtained from the classical results given in Sec. III shows that γ_2 and γ_3 are within 20% of the same value. Thus, to a fair approximation, germanium may be assumed to have $\gamma_2=\gamma_3=\bar{\gamma}$. Cyclotron resonance in this "germaniumlike" crystal may now be considered to see if the $P_H=0$ assumption holds since solutions of (1) may be found for both $P_H=0$ and $P_H\neq 0$. For convenience the orientation of the magnetic field will be along the [111] direction. Using methods identical with those in JML, **P** and **J** are rotated in order to get one component of **P** along **H**. The q in JML has been estimated to be

* This paper is based on a thesis submitted to the University of Michigan in partial fulfillment of the requirements for a Ph.D. degree.

† Now at Colorado State University, Fort Collins, Colorado.

[1] See R. Peierls, Z. Physik **80**, 736 (1933); **81**, 186 (1933); G. H. Wannier, Phys. Rev. **52**, 191 (1937); J. C. Slater, Phys. Rev. **76**, 1592 (1949).

[2] G. Dresselhaus, A. F. Kip, and C. Kittel, Phys. Rev. **92**, 827 (1953); **95**, 568 (1954); R. N. Dexter, H. J. Zeiger, and B. Lax, *ibid.* **95**, 557 (1954). Throughout this paper reference to these papers will be made as DKK and DZL.

[3] W. Shockley, Phys. Rev. **78**, 173 (1950).

[4] J. M. Luttinger, Phys. Rev. **102**, 1030 (1956). This reference will be referred to as JML throughout this paper.

[5] W. Shockley, Phys. Rev. **90**, 491 (1953).

[6] J. M. Luttinger and W. Kohn, Phys. Rev. **97**, 869 (1955). This paper will be referred to as LK throughout the remainder of this paper.

[7] R. C. Fletcher, W. A. Yaeger, and F. R. Merritt, Phys. Rev. **100**, 747 (1955). This paper will be referred to as FYM throughout the remainder of this paper.

[8] J. M. Luttinger and R. R. Goodman, Phys. Rev. **100**, 673 (1955).

~ 0.01 by Kohn[9] and will be omitted. The final matrix D is given by

$$-\frac{mc}{eH}D=\begin{bmatrix} (\gamma_1+\bar{\gamma})(a^\dagger a+\frac{1}{2})+\frac{3}{2}\kappa & -\sqrt{3}\bar{\gamma}a^2 & -(6)^{\frac{1}{2}}\bar{\gamma}P_H a & 0 \\ +\frac{1}{2}(\gamma_1-2\bar{\gamma})P_H^2 & & & \\ -\sqrt{3}\bar{\gamma}(a^\dagger)^2 & (\gamma_1-\bar{\gamma})(a^\dagger a+\frac{1}{2})-\frac{1}{2}\kappa & 0 & (6)^{\frac{1}{2}}\bar{\gamma}P_H a \\ & +\frac{1}{2}(\gamma_1+2\bar{\gamma})P_H^2 & & \\ -(6)^{\frac{1}{2}}\bar{\gamma}P_H a^\dagger & 0 & (\gamma_1-\bar{\gamma})(a^\dagger a+\frac{1}{2})+\frac{1}{2}\kappa & -\sqrt{3}\bar{\gamma}a^2 \\ 0 & (6)^{\frac{1}{2}}\bar{\gamma}P_H a^\dagger & -\sqrt{3}\bar{\gamma}(a^\dagger)^2 & (\gamma_1+\bar{\gamma})(a^\dagger a+\frac{1}{2})-\frac{3}{2}\kappa \\ & & & +\frac{1}{2}(\gamma_1-2\bar{\gamma})P_H^2 \end{bmatrix}, \quad (2)$$

where a factor $-eH/mc$ has been omitted. This only affects the units of measure of energy in cyclotron resonance analysis. The solutions are of the form

$$\psi_m=\begin{bmatrix} C_m{}^1 u_{m-3} \\ C_m{}^2 u_{m-1} \\ C_m{}^3 u_{m-2} \\ C_m{}^4 u_m \end{bmatrix}, \quad (3)$$

where all symbols are the same as those given in JML except $\mathbf{k}$ is given here by $\mathbf{P}$. For $m<3$ the solutions are subject to the conditions

$$\begin{aligned} &m=0: \quad C_0{}^1=C_0{}^2=C_0{}^3=0; \\ &m=1: \quad C_1{}^1=C_1{}^3=0; \\ &m=2: \quad C_2{}^1=0. \end{aligned} \quad (4)$$

Using the properties of the creation and annihilation operators $a^\dagger$ and a operating on the harmonic oscillator wave functions u_m and substituting (2) and (3) into (1), a set of determinantal equations are obtained for the determination of the energy levels E_m. For each $m\geq 3$, there are four values of E_m. Thus it is necessary to label each E_m with another index ρ ($\rho=1, 2, 3, 4$). For $m=2$, $\rho=1, 2, 3$; for $m=1$, $\rho=1, 2$; and, for $m=0$, there is only one E_0. The convention chosen here for $E_{m,\rho}$ is that $E_{m,1}<E_{m,2}<E_{m,3}<E_{m,4}$. These determinantal equations may be computed numerically by electronic computers. The special case $P_H=0$ which also is of interest here is seen to be identical with that considered in Luttinger's paper simply by setting $P_H=0$ in (2) and comparing the matrix to Luttinger's Eq. (71). The labeling of levels in Luttinger's paper is different from that used here, however.

The energy levels and the wave functions are now known for both $P_H=0$ and $P_H\neq 0$. It remains to compare the absorption line shapes for both cases. In order to do this we make use of the equation for the absorption line shape derived in Appendix A. All quantities appearing in the line shape Eq. (A21) are in principle known. The matrix elements may be expressed using Eq. (2) as

$$y_{m,\rho;m+1,\sigma}=\frac{1}{\sqrt{2}\omega_0}[C_{m,\rho}{}^1 C_{m+1,\sigma}{}^1(m-2)^{\frac{1}{2}}+C_{m,\rho}{}^2 C_{m+1,\sigma}{}^2\sqrt{m} +C_{m,\rho}{}^3 C_{m+1,\sigma}{}^3(m-1)^{\frac{1}{2}}+C_{m,\rho}{}^4 C_{m+1,\sigma}{}^4(m+1)^{\frac{1}{2}}] \quad (5)$$

where $\omega_0=eH/mc$. Thus if the integration in (A21) is to be performed, it is necessary to obtain the energy levels $E_{m,\rho}$ as well as the coefficients in the eigenfunction (3). In general this requires the solution of quartic equations. The integrals, being too complicated to perform in general, were done numerically. The IBM 650 digital computer was programmed to find the $E_{m,\rho}$ and $C_{m,\rho}{}^i$ as a function of P_H. Several transitions were considered.

Before presenting the numerical results, it is of interest to consider the types of transitions which are possible for both the $P_H=0$ and $P_H\neq 0$ cases. It has already been shown that transitions may occur only if the final state differs from the initial state by ± 1 in the quantum number m. This must be true for both cases. In the $P_H=0$ case transitions between any of the four levels associated with m and those with $m\pm 1$. Some of these transitions turn out to be relatively improbable. For the $P_H=0$ case, these same selection rules do not hold. Setting $P_H=0$ splits the Hamiltonian into two independent 2×2 matrices. This automatically eliminates transitions between the levels of one 2×2 matrix and those of the other 2×2 matrix. The $P_H\neq 0$ tends to allow these forbidden transitions. (In JML's notation for energy levels for $P_H=0$, the transitions which are allowed for $P_H\neq 0$ but forbidden for $P_H=0$ are these between the ladders $\epsilon_1{}^{\pm}(n)$ and $\epsilon_2{}^{\pm}(n)$.) Since a comparison of line shapes for $P_H=0$ and $P_H\neq 0$ is desired, only transitions which are allowed for both schemes will be considered.

For the purpose of comparison a typical transition was chosen and the absorption curve for $P_H=0$ was calculated for comparison with the calculated curve for $P_H\neq 0$. Using the method outlined above, the typical values of the effective-mass constants used were

$$\gamma_1=13.2, \quad \bar{\gamma}=4.4, \quad \kappa=4.0.$$

The transition $m=2, \rho=1 \rightarrow m=3, \rho=2$ was con-

[9] W. Kohn (private communication).

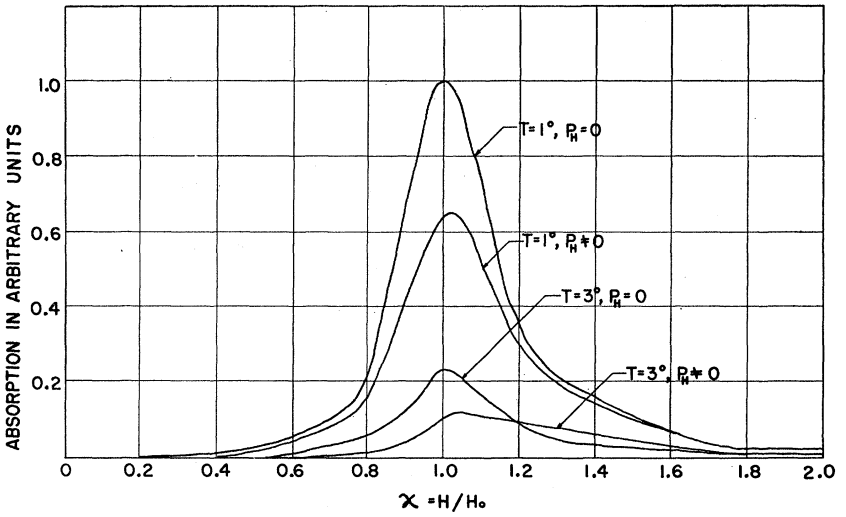

FIG. 1. The line shapes for $m=2,\rho=1\rightarrow m=3,\rho=2$; $T=1°$K, 3°K.

sidered. The integration of the line-shape equation (A21) as well as the determination of the eigenvalues and eigenfunctions were done on the IBM 650 computer. Calculations were performed using the parameters

$$\omega=1.5\times10^{11}\text{ rad/sec},$$
$$(\omega\tau)^2=57,$$
$$T=1°\text{ and }3°\text{K}.$$

The numerical results are plotted along with the $P_H=0$ results in Fig. 1. From Fig. 1 it is seen that the shift in the absorption peak is less than 2% when $P_H=0$ is assumed. Thus, the type of transition which is allowed for both $P_H=0$ and $P_H\neq0$ may be found with little error by using the much simpler $P_H=0$ calculations. It is true that only one transition of this type was considered here; however, remembering that the classical absorption curves, or higher quantum transitions, are not shifted significantly by setting $P_H=0$, it seems reasonable that none of these transitions will be affected appreciably.

One of the transitions allowed for $P_H\neq0$ and forbidden for $P_H=0$ was investigated. The transition line shape for $m=0,\rho=1\rightarrow n=1,\sigma=1$ was calculated and found to be of an entirely different character than the one presented above. It was found to be very temperature dependent and highly asymmetric. The "P_H-induced" type transition is, therefore, easily distinguished from the $P_H=0$ transitions. It is also estimated to have a relative intensity to the normal absorption curve of less than 10%. Figure 2 shows the line shape for this "P_H-induced" transition.

III. DETERMINATION OF THE EFFECTIVE-MASS CONSTANTS

With the validity of the $P_H=0$ assumption verified, it is now possible to continue on with the cyclotron resonance analysis. As mentioned earlier, it is possible to find solutions to (1) for the $P_H=0$ case when the magnetic field is in the [111] direction. The other directions may be handled by approximation methods. It is the results of these calculations which will allow comparison with experiment. The experiments chosen were those of FYM. The values of γ_1, γ_2, γ_3, and κ were varied until a best fit of their data was obtained. The experiments of FYM were done at two temperatures: 4.2° and 1.3°K. In order to obtain estimates of these constants, the 4.2°, or "classical" case, was analyzed first. For this case the equations of DKK are valid. They showed that the cyclotron resonance frequencies in the valence band for Ge are given by

$$\omega^{\pm}(\theta)=2\pi\Big/\int_0^{2\pi}d\phi\{A\pm[B^2+\tfrac{1}{4}C^2(1+g(\phi))]^{\frac{1}{2}}\}^{-1},\quad(6)$$

where

$$g(\phi)=(1-3\cos^2\theta)\{(\cos^2\theta-3)\cos^4\phi+2\cos^2\phi\}\quad(7)$$

and θ is the angle of the magnetic field in the (110) plane measured from the [001] axis. Equation (6) may be expressed in terms of complete elliptic integrals of the first and third kind. Since the existing tables for the elliptic integrals of the third kind are too incomplete to be of use here, Eq. (6) was expanded in terms of $g(\phi)$ and integrated term by term. For **H** in the [001], [111], and [100] directions, (6) may be written as

$$\omega^{\pm}[111]=A\pm(B^2+\tfrac{1}{4}C^2)^{\frac{1}{2}}$$
$$\omega^{\pm}[100]\cong\omega^{\pm}[111]\Big/\left\{1\pm\frac{C^2}{16\omega^{\pm}[111](B^2+\tfrac{1}{4}C^2)^{\frac{1}{2}}}\right\}\quad(8)$$
$$\omega^{\pm}[110]\cong\omega^{\pm}[111]\Big/\left\{1\pm\frac{C^2}{64\omega^{\pm}[111](B^2+\tfrac{1}{4}C^2)^{\frac{1}{2}}}\right\}.$$

By using the values of $\omega^{\pm}$ given in FYM for 4.2°, the constants A, B, and C may be determined. The values

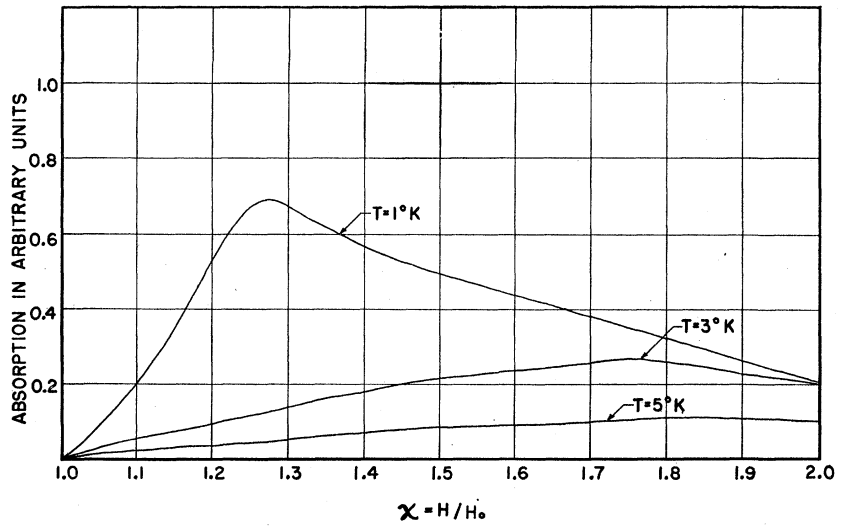

FIG. 2. The line shapes for the "P_H-induced" transition $m=0$, $\rho=1 \rightarrow m=1$, $\rho=1$.

$\omega^+[111]=23.75$, $\omega^-[111]=2.66$, and $\omega^+[100]=22.88$ give

$$A=13.21, \quad B^2=73.03, \quad \tfrac{1}{4}C^2=38.06. \tag{9}$$

Using these values in $\omega^-[100]$ and $\omega^\pm[110]$ and evaluating them serves as a check, giving results in good agreement with the values given in FYM. Using JML's identities these constants give

$$\gamma_1=13.21, \quad \gamma_2=4.28, \quad \gamma_3=5.56. \tag{10}$$

The γ_2 and γ_3 must be considered as only rough estimates due to the approximations used in handling the expansions of (8). In order to obtain a value for $C^2/4$, it is the difference between the experimental values $\omega^+[111]$, $\omega^+[100]$, and $\omega^+[110]$ which must be used. It may be seen in FYM that the values of ω^+ do not differ by much and, therefore, small experimental error shows an appreciable variation in the value of $C^2/4$. If the experimental values of ω^- are used, the corresponding series converge very slowly.

For the purpose of comparing the quantum results with FYM's experiments at 1.3°, the values of γ_2 and γ_3 may be varied about the values given in (11). Using transformations similar to the one used in the previous section and taking $P_H=0$, it is possible to obtain the desired Hamiltonians for the [110] and [100] cases. The Hamiltonian for the [111] case is obtained by setting $P_H=0$ in Eq. (2). These three cases are then given by the Hamiltonians:

$$D_{100}=\begin{pmatrix} (\gamma_1+\gamma_2)(a^\dagger a+\frac{1}{2})+\frac{3}{2}\kappa & \frac{1}{2}\sqrt{3}\{(\gamma_2-\gamma_3)(a^\dagger)^2 & 0 & 0 \\ & +(\gamma_2+\gamma_3)a^2\} & & \\ \frac{1}{2}\sqrt{3}\{(\gamma_2-\gamma_3)a^2 & (\gamma_1-\gamma_2)(a^\dagger a+\frac{1}{2})-\frac{1}{2}\kappa & 0 & 0 \\ +(\gamma_2+\gamma_3)(a^\dagger)^2\} & & & \\ 0 & 0 & (\gamma_1-\gamma_2)(a^\dagger a+\frac{1}{2})+\frac{1}{2}\kappa & \frac{1}{2}\sqrt{3}\{(\gamma_2-\gamma_3)(a^\dagger)^2 \\ & & & +(\gamma_2+\gamma_3)a^2\} \\ 0 & 0 & \frac{1}{2}\sqrt{3}\{(\gamma_2-\gamma_3)a^2 & (\gamma_1+\gamma_2)(a^\dagger a+\frac{1}{2})-\frac{3}{2}\kappa \\ & & +(\gamma_2+\gamma_3)(a^\dagger)^2\} & \end{pmatrix} \tag{11}$$

$$D_{111}=\begin{pmatrix} (\gamma_1+\gamma_3)(a^\dagger a+\frac{1}{2})+\frac{3}{2}\kappa & -(1/\sqrt{3})(\gamma_2+2\gamma_3)a^2 & -(\frac{2}{3})^{\frac{1}{2}}(\gamma_3-\gamma_2)(a^\dagger)^2 & 0 \\ -(1/\sqrt{3})(\gamma_2+2\gamma_3)(a^\dagger)^2 & (\gamma_1-\gamma_3)(a^\dagger a+\frac{1}{2})-\frac{1}{2}\kappa & 0 & (\frac{2}{3})^{\frac{1}{2}}(\gamma_3-\gamma_2)(a^\dagger)^2 \\ -(\frac{2}{3})^{\frac{1}{2}}(\gamma_3-\gamma_2)a^2 & 0 & (\gamma_1-\gamma_3)(a^\dagger a+\frac{1}{2})+\frac{1}{2}\kappa & -(1/\sqrt{3})(\gamma_2+2\gamma_3)a^2 \\ 0 & (\frac{2}{3})^{\frac{1}{2}}(\gamma_3-\gamma_2)a^2 & -(1/\sqrt{3})(\gamma_2+2\gamma_3)(a^\dagger)^2 & (\gamma_1+\gamma_3)(a^\dagger a+\frac{1}{2})-\frac{3}{2}\kappa \end{pmatrix} \tag{12}$$

$$D_{110}=\begin{pmatrix} (\gamma_1+\frac{1}{4}\gamma_2+\frac{3}{4}\gamma_3)(a^\dagger a+\frac{1}{2})+\frac{3}{2}\kappa & \frac{1}{4}\sqrt{3}\{(\gamma_3-\gamma_2)[a^\dagger a+\frac{1}{2}+\frac{3}{2}(a^\dagger)^2] & 0 & 0 \\ -\frac{3}{8}(\gamma_3-\gamma_2)(a^2+(a^\dagger)^2) & -\frac{1}{2}(3\gamma_2+5\gamma_3)a^2\} & & \\ \frac{1}{4}\sqrt{3}\{(\gamma_3-\gamma_2)(a^\dagger a+\frac{1}{2}+\frac{3}{2}a^2) & (\gamma_1-\frac{1}{4}\gamma_2-\frac{3}{4}\gamma_3)(a_2a+\frac{1}{2})-\frac{1}{2}\kappa & 0 & 0 \\ -\frac{1}{2}(3\gamma_2+5\gamma_3)(a^\dagger)^2\} & +\frac{3}{8}(\gamma_3-\gamma_2)(a^2+(a^\dagger)^2) & & \\ 0 & 0 & (\gamma_1-\frac{1}{4}\gamma_2-\frac{3}{4}\gamma_3)(a^\dagger a+\frac{1}{2})+\frac{1}{2}\kappa & \frac{1}{4}\sqrt{3}\{(\gamma_3-\gamma_2)[a^\dagger a+\frac{1}{2}+\frac{3}{2}(a^\dagger)^2] \\ & & +\frac{3}{8}(\gamma_3-\gamma_2)[a^2+(a^\dagger)^2] & -\frac{1}{2}(3\gamma_2+5\gamma_3)a^2 \\ 0 & 0 & \frac{1}{4}\sqrt{3}\{(\gamma_3-\gamma_2)(a^\dagger a+\frac{1}{2}+\frac{3}{2}a^2) & (\gamma_1+\frac{1}{4}\gamma_2+\frac{3}{4}\gamma_3)(a^\dagger a+\frac{1}{2})-\frac{3}{2}\kappa \\ & & -\frac{1}{2}(3\gamma_2+5\gamma_3)(a^\dagger)^2\} & -\frac{3}{8}(\gamma_3-\gamma_2)[a^2+(a^\dagger)^2] \end{pmatrix}. \tag{13}$$

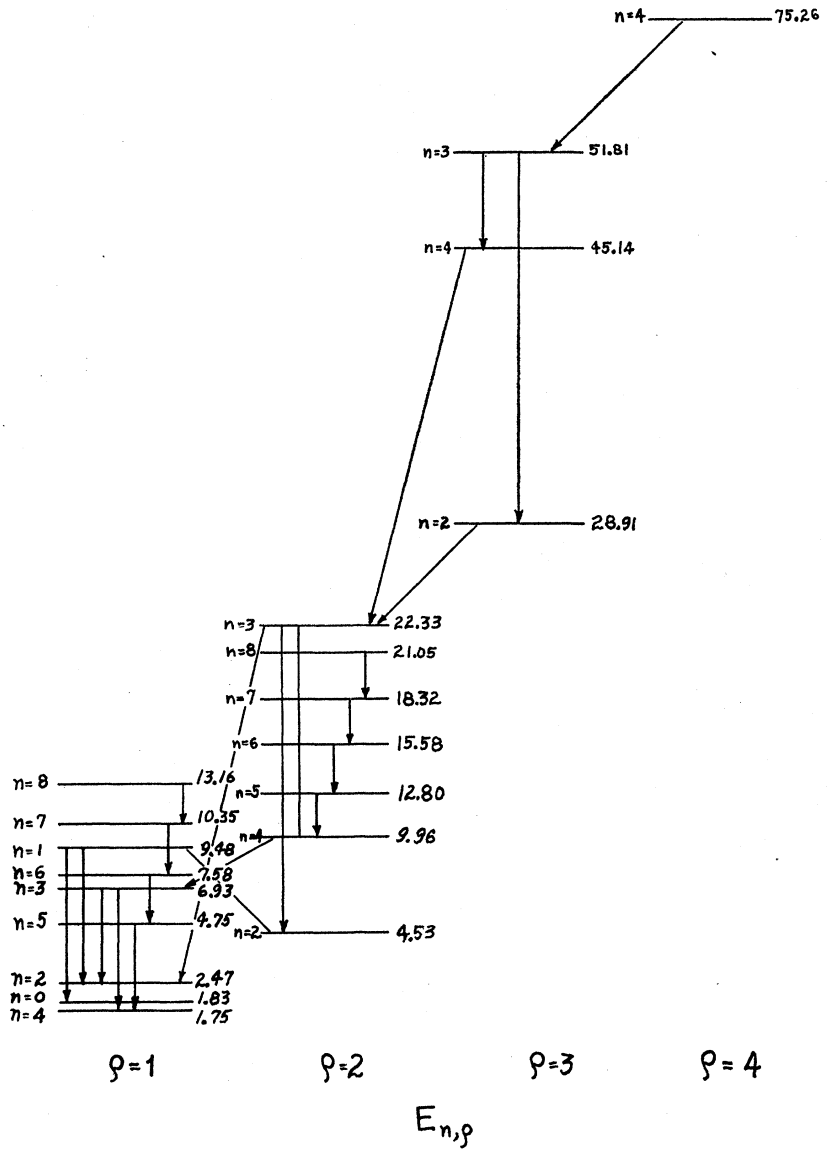

FIG. 3. Energy level diagram for [111] direction.

The only one of these Hamiltonians which has a known exact eigensolution is the D_{111}. Upon inspection of (12) it is seen that the solution for the wave function is

$$\psi_n=\begin{pmatrix} C_n{}^1u_{n-2} \\ C_n{}^2u_n \\ C_n{}^3u_{n-4} \\ C_n{}^4u_{n-2} \end{pmatrix}. \tag{14}$$

For $n=0, 1$ it is understood that $C_n{}^1=C_n{}^3=C_n{}^4=0$, and for $n=2, 3$ that $C_n{}^3=0$. The equation for the eigenvalues of E_n of the Schrödinger equation for $n\geqslant 4$ is given by a 4×4 determinant. For $n=0, 1$ the energy is given by

$$E_n=(\gamma_1-\gamma_3)(n+\tfrac{1}{2})-\tfrac{1}{2}\kappa. \tag{13}$$

A 3×3 determinant is found for $n=2, 3$. By varying the values of γ_2, γ_3, and κ, it is possible to get values of the energy from these equations which, with the help of the selection rules for harmonic oscillator wave functions, may be fitted to the data of FYM. The selection rules for dipole transitions allow only $\Delta n=\pm 1$. Energy levels were calculated by the use of an IBM 650 for the range of values $5.4\leqslant\gamma_3\leqslant 5.7$ and $3.7\leqslant\kappa\leqslant 4.2$. The value of γ_1 was fixed at 13.21 and γ_2 was determined by

$$\gamma_2=[(10.54)^2-3\gamma_3{}^2]^{\frac{1}{2}}, \tag{14}$$

which follows from the classical analysis. The values of κ were chosen near Kohn's[9] estimate $\kappa=4$. The energy levels of a typical calculation appear in Fig. 3. Some of the allowed transitions are indicated by the arrows. All values of γ_3 between 5.4 and 5.6 give good agreement for the resonant peaks $\omega=3.01$, 2.78, and 2.60

found by FYM. Other transitions are sensitive to variations in γ_3 and κ such as $n=3,\rho=1\rightarrow n=2,\rho=1$; $n=3,\rho=1\rightarrow n=2,\rho=2$; $n=1,\rho=1\rightarrow n=2,\rho=2$. Three sets of values of γ_3 and κ are found which give best agreement with FYM. These are

$$\begin{aligned}&\gamma_3=5.55\pm0.02,\quad \kappa=3.9\pm0.1\\&\gamma_3=5.60\pm0.02,\quad \kappa=3.9\pm0.1\\&\gamma_3=5.61\pm0.02,\quad \kappa=4.2\pm0.1.\end{aligned}\tag{15}$$

Table I indicates the experimental resonant frequencies and those given by theory for the above values of γ_3 and κ. Even these values do not predict all peaks observed by FYM, and they all predict additional peaks not observed. More will be said concerning this later. These three sets of values may now be used in either the [100] or [110] cases to determine which fits the data best. The [100] direction is considered next. It has already been mentioned that an exact solution to (11) is not known. It may be noticed, however, that the Hamiltonian contains terms with coefficients $\gamma_2+\gamma_3$ and $\gamma_2-\gamma_3$. Since it may be roughly estimated from the classical results that $(\gamma_3-\gamma_2)/(\gamma_3+\gamma_2)\sim0.1$ it is possible to consider the $(\gamma_2-\gamma_3)$ terms as a perturbation in the problem. Writing

$$D_{100}=D_0+D_1\tag{16}$$

where

$$D_0=\begin{bmatrix}(\gamma_1+\gamma_2)(a^\dagger a+\frac{1}{2})+\frac{3}{2}\kappa & \frac{1}{2}\sqrt{3}(\gamma_2+\gamma_3)a^2 & 0 & 0\\ \frac{1}{2}\sqrt{3}(\gamma_2+\gamma_3)(a^\dagger)^2 & (\gamma_1-\gamma_2)(a^\dagger a+\frac{1}{2})-\frac{1}{2}\kappa & 0 & 0\\ 0 & 0 & (\gamma_1-\gamma_2)(a^\dagger a+\frac{1}{2})+\frac{1}{2}\kappa & \frac{1}{2}\sqrt{3}(\gamma_2+\gamma_3)a^2\\ 0 & 0 & \frac{1}{2}\sqrt{3}(\gamma_2+\gamma_3)(a^\dagger)^2 & (\gamma_1+\gamma_2)(a^\dagger a+\frac{1}{2})-\frac{3}{2}\kappa\end{bmatrix}\tag{17}$$

is the zeroth-order Hamiltonian and the perturbation term is

$$D_1=-\tfrac{1}{2}\sqrt{3}(\gamma_3-\gamma_2)\begin{bmatrix}0 & (a^\dagger)^2 & 0 & 0\\ a^2 & 0 & 0 & 0\\ 0 & 0 & 0 & (a^\dagger)^2\\ 0 & 0 & a^2 & 0\end{bmatrix}\tag{18}$$

it is seen that the problem reduces to two 2×2 perturbation problems. Solutions are easily found for the zeroth order equations. (Each is a 2×2.) These are

$$\psi_n{}^{(1)}=\begin{pmatrix}a_n{}^1u_{n-2}\\ a_n{}^2u_n\end{pmatrix},\quad \psi_n{}^{(2)}=\begin{pmatrix}b_n{}^1u_{n-2}\\ b_n{}^2u_n\end{pmatrix},\tag{19}$$

where the (1) and (2) refer to the upper 2×2 and lower 2×2 matrix, respectively. Numerical solutions of the second order perturbation were made for the energy levels by the use of a computer for the values of the γ_3 and κ given above. The best fit to the FYM data is given by $5.60\pm0.02=\gamma_3$ and $\kappa=4.0\pm0.2$. Table II shows results of these calculations as compared to FYM. For $\gamma_3=5.60\pm0.02$ all observed peaks are accounted for except $\omega=3.17$ and 3.34. Most transitions are relatively insensitive to variations in κ, thus its value could not be narrowed down by the [100] analysis.

In order to verify this choice of γ_3, it was used in the [110] analysis. The other constants were taken to be $\gamma_1=13.21$ and $\kappa=3.8$. The [110] solutions may be obtained by a second-order perturbation exactly analogous to the [100] case. Numerical results show good agreement for the resonant peaks 3.21, 2.91, and 2.72 of FYM. The peak at 3.83 may be accounted for by one transition which is predicted near 4.01 but is extremely sensitive to small variations in γ_3. Again a variation in κ may be shown not to give significant changes in the predicted frequencies. The results do not conflict with the choice of γ_3. Thus the best set of values are given by

$$\gamma_1=13.2,\quad \gamma_2=4.1,\quad \gamma_3=5.6,\quad \kappa=3.9.$$

TABLE I. A list of lines predicted which account for the observed lines of FYM.

Resonant freq. found by FYM [111] direction at $T=1.3°K$	Predicted by $\gamma_3=5.55\pm0.02$ $\kappa=3.9$	$\gamma_3=5.60\pm0.02$ $\kappa=3.9$	$\gamma_3=5.61\pm0.02$ $\kappa=4.2$
2.25(?)	NP[a]	2.16±0.10	2.25±0.07
2.47	2.43±0.07	NP	NP
2.66	2.69	2.69	2.69
2.78	2.78	2.78	2.78
	2.99	2.97	2.97
3.01	3.03	3.03	3.04
3.22	NP	NP	NP
3.94(?)	NP	NP	NP
4.37(?)	4.37±0.12	4.78±0.20(?)	4.56±0.12
23.75	23.69[b]	23.71[b]	23.71[b]

[a] NP = not predicted.
[b] Many lines are also predicted in this region.

TABLE II. A list of lines predicted which account for the observed lines of FYM.

Observed by FYM	$\gamma_3=5.55\pm0.02$	$\gamma_3=5.60+0.02$
1.69	NP[a]	2.00 ±0.30
2.71	NP	2.56 ±0.12
3.17(?)	NP	NP
3.34	NP	NP
3.59	3.60±0.05[b]	3.65 ±0.05[b]
4.20	4.00±0.20(?)	4.20 ±0.12[b]
4.76	NP	4.68 ±0.030
17.54±0.60	18.09±0.08	18.26 ±0.08
22.88	22.70±0.26	22.06[b]±0.26

[a] NP = not predicted.
[b] Many lines are predicted near this value.

IV. DISCUSSION

The above values of $\gamma_1\gamma_2\gamma_3$ and κ are subject to error for several reasons. Experimental error in FYM's measurements is probably of the order of 1%. The $P_H=0$ assumption causes an error which is estimated to be no larger than 1%. Additional error is introduced in the perturbation calculations in the [100] and [110] cases. The error of this is estimated to be of the order of 2%. Since none of the values of γ_3 and κ fit the data completely, the possibility of other values, say $\gamma_3=5.55$, which also fit some of the peaks may not be altogether excluded.

From Fig. 3 it may be seen that some transitions are predicted which are not observed in FYM. Experimental limitations could account for this. One such line is the transition from $n=1, \rho=1 \rightarrow n=0, \rho=1$, which, from Eq. (13), may be shown to have a frequency

$$\omega=(\gamma_1-\gamma_3)$$

and is, therefore, estimated to $\omega=7.6$. The observation of this transition would simplify the analysis since it has such a simple functional dependence on γ_1 and γ_3. Since the value of γ_1 is well established, it would immediately determine γ_3. Similar transitions occur for the [100] direction ($\omega\cong 8.9$) and for the [110] direction ($\omega\cong 9.0$) of magnetic field. There is a possibility that this line was observed by Dousmanis *et al.*[10] in an unaccounted-for peak in their negative-mass cyclotron resonance experiments.

Some lines appear in FYM which are not predicted here. Some of these such as in the [100] case possibly could be due to the P_H-induced lines previously mentioned. If this is the case they could easily be identified, since P_H-induced lines are strongly temperature dependent, by a small change in temperature. The exact location of these peaks at a given temperature is difficult to determine numerically. Since in general P_H-induced lines are not strong, it is difficult to see how they could account for a strong transition such as $\omega=3.34$ in the [100] data.

More detailed analysis is plausible when more complete experiments have been performed at a number of temperatures. This would allow identification of P_H-induced lines, if any exist, and also give information concerning the population of levels at different temperatures. Hensel and Martin[11] have recently suggested that Stark shifts are plausible as a means of identifying cyclotron resonance transitions. An identification of transitions would greatly simplify the analysis.

ACKNOWLEDGMENTS

The author would like to thank Dr. J. M. Luttinger for suggesting the topic and for his assistance throughout the course of this work. He would also like to thank Mr. Marshall Pines for his patient help in the numerical computations done at the University of Michigan Computing Center.

APPENDIX A

The quantum theory of line broadening is presented in this Appendix for the purpose of obtaining a line-shape equation. The mechanism for the line broadening is assumed to be, for simplicity, that of a simple collision which has a relaxation time τ. The formalism used here is similar to that of Karplus and Schwinger.[12]

We begin by considering an oscillating electric field which perturbs a system which has an original Hamiltonian $\mathcal{H}_0$. The electric field is given by

$$\mathbf{E}(t)=\mathbf{E}^0\cos\omega t, \tag{A1}$$

where $\mathbf{E}^0$ is a constant vector. The Hamiltonian which includes the perturbation may be given by

$$\mathcal{H}=\mathcal{H}_0+\frac{e}{\omega}\mathbf{E}^0\cdot\mathbf{v}\sin\omega t, \tag{A2}$$

where $\mathbf{v}$ is the velocity of the system. The gauge chosen here is

$$\frac{1}{C}\frac{\partial}{\partial t}\mathbf{A}=-\mathbf{E}^0\cos\omega t.$$

We wish to calculate the power absorbed per unit volume, which is easily seen to be

$$\mathcal{P}=ne\{\langle v_\alpha(t)\rangle E_\alpha(t)\}_t, \tag{A3}$$

where $\{\ \}_t$ indicates an average over time and $\langle\ \rangle$ indicates an averaging over the time of the last collision as well as a Boltzmann averaging. Thus

$$\langle v_\alpha(t)\rangle=\sum_j\sum_m (v_\alpha)_{mj}(\bar{\rho}(t))_{jm}, \tag{A4}$$

where $\bar{\rho}(t)$ is the density matrix averaged over the time of the last collision. It is the $(\bar{\rho}(t))_{jm}$ which must be calculated before (A3) can be written in an explicit form. The precise meaning of this quantity will become clear in the next paragraph.

To begin with, the strong collision assumption is made. Assume that such a collision occurred at a time t_0. Complete equilibrium, being reached immediately after the collision, allows the density matrix for $t=t_0$ to be written

$$\rho(t_0)=\exp[-\beta\mathcal{H}(t_0)]/\mathrm{Tr}\exp[-\beta\mathcal{H}(t_0)]. \tag{A5}$$

It is also true that

$$i\hbar\partial\rho/\partial t=[\mathcal{H},\rho], \tag{A6}$$

where $[\ ,\ ]$ is the commutator. The density matrix at some time t clearly depends on t and t_0. The value of ρ then must be averaged over all t_0. Call this averaged quantity $\bar{\rho}$. If the probability that a collision last

[10] G. C. Dousmanis, R. C. Duncan, J. J. Thomas, and R. C. Williams, Phys. Rev. Letters **1**, 404 (1958).

[11] J. C. Hensel and Martin Peter, Phys. Rev. **114**, 411 (1959).

[12] R. Karplus and J. Schwinger, Phys. Rev. **73**, 1020 (1948).

occurred in the interval $t-\vartheta$ to $t-\vartheta+d\vartheta$ is given by

$$\frac{d\vartheta}{\tau}e^{-\vartheta/\tau}$$

then

$$\bar{\rho}(t)=\int_{0}^{\infty}\frac{1}{\tau}\rho(t,t-\vartheta)e^{-\vartheta/\tau}d\vartheta. \tag{A7}$$

It is easily shown from this that

$$\frac{\partial\bar{\rho}}{\partial t}=\frac{1}{i\hbar}[\mathcal{H},\bar{\rho}]-\frac{1}{\tau}\int_{0}^{\infty}\frac{\partial\rho(t,t-\vartheta)}{\partial\vartheta}e^{-\vartheta/\tau}d\vartheta. \tag{A8}$$

If the integral is integrated by parts

$$\frac{\partial\bar{\rho}}{\partial t}=\frac{1}{i\hbar}[\mathcal{H},\bar{\rho}]-\frac{1}{\tau}(\bar{\rho}(t)-\rho_0(t)), \tag{A9}$$

where

$$\rho_0(t)\equiv\rho(t,t). \tag{A10}$$

Integration of (A9) is now necessary. Define the deviation of $\bar{\rho}$ from ρ as

$$D\equiv\bar{\rho}(t)-\rho_0(t). \tag{A11}$$

If a representation is chosen such that the unperturbed Hamiltonian $\mathcal{H}_0$ is diagonal, it is easily seen that Eq. (A9) yields, in matrix language,

$$\frac{\partial D_{mn}}{\partial t}+\left(i\omega_{mn}+\frac{1}{\tau}\right)D_{mn}=-\frac{\partial}{\partial t}(\rho_0(t))_{mn}-\frac{ie}{\omega\hbar}\sum_i[(\mathbf{E}^0\cdot\mathbf{v})D_{jn}-D_{mj}(\mathbf{E}^0\cdot\mathbf{v})_{jn}]\sin\omega t, \tag{A12}$$

where

$$\omega_{mn}=(1/\hbar)(E_m^{(0)}-E_n^{(0)}). \tag{A13}$$

The $E_n^{(0)}$ are the unperturbed energy eigenvalues. Using perturbation methods the density matrix to first order may be written

$$(\rho_0(t))_{mn}=\rho_m^{(0)}\delta_{mn}\left(1-\frac{\beta e}{\omega}(\mathbf{E}^0\cdot\mathbf{v})_{mn}\sin\omega t\right)+\frac{\rho_m^{(0)}-\rho_n^{(0)}}{\hbar\omega_{mn}}\frac{e}{\omega}(\mathbf{E}^0\cdot\mathbf{v})_{mn}\sin\omega t. \tag{A14}$$

This step follows directly from the method given in Appendix I in Karplus and Schwinger.[12] The term $\rho_m^{(0)}$ is the unperturbed density matrix given by

$$\rho^{(0)}=\exp[-\beta\mathcal{H}_0]/\mathrm{Tr}\exp[-\beta\mathcal{H}_0]. \tag{A15}$$

The last term in (A12) is clearly of second order in the perturbation, so to first order it may be omitted. Combining (A12), (A14), and (A15) and considering the steady-state case, we may write

$$(\bar{\rho}(t))_{mn}=\rho_m^{(0)}\delta_{mn}+\frac{e}{2}(\mathbf{E}^0\cdot\mathbf{v})_{mn}\left(\beta\rho_m^{(0)}\delta_{mn}-\frac{\rho_m^{(0)}-\rho_n^{(0)}}{\hbar\omega_{mn}}\right)\times\left\{\left(\frac{\tau}{1+i\tau(\omega+\omega_{mn})}-\frac{1}{i\omega}\right)e^{i\omega t}+\left(\frac{\tau}{1+i\tau(\omega_{mn}-\omega)}+\frac{1}{i\omega}\right)e^{-i\omega t}\right\}. \tag{A16}$$

With this explicit form of $\bar{\rho}(t)$ it is now possible to perform the time average in the equation for the power absorption. Considering, of course, only the real part of the result, (A3) becomes

$$\mathcal{P}=\tfrac{1}{4}ne^2\tau E_\alpha^0E_\gamma^0\left\{\frac{2\beta}{1+(\omega\tau)^2}\sum_m(v_\alpha)_{mm}(v_\gamma)_{mm}\rho_m^{(0)}-\sum_{m,n}{}'(v_\alpha)_{mn}(v_\gamma)_{mn}\frac{\rho_m^{(0)}-\rho_n^{(0)}}{\hbar\omega_{mn}}\times\left(\frac{1}{1+\tau^2(\omega+\omega_{mn})^2}+\frac{1}{1+\tau^2(\omega-\omega_{mn})^2}\right)\right\}. \tag{A17}$$

The α and γ are the vector component indices. If the special case where the electric vector $\mathbf{E}^0$ is directed along the y axis is considered, the simplified result

$$\mathcal{P}=\tfrac{1}{4}ne^2\tau(E^0)^2\left\{\frac{2\beta}{1+(\omega\tau)^2}\sum_m(v_y)_{mm}{}^2\rho_m^{(0)}-\sum_{m,n}{}'(v_y)_{mn}{}^2\frac{\rho_m^{(0)}-\rho_n^{(0)}}{\hbar\omega_{mn}}\times\left(\frac{1}{1+\tau^2(\omega+\omega_{mn})^2}+\frac{1}{1+\tau^2(\omega-\omega_{mn})^2}\right)\right\} \tag{A18}$$

is obtained. It is this equation that is to be modified to our needs. The summation must be extended to include a summation over the index ρ (discussed in Sec. III) as well as the quantum number n. An integration over P_H must also be included. Considerable simplification occurs when, using the relation

$$(v_\alpha)_{mn}=(i/\hbar)[\mathcal{H},x_\alpha]_{mn}$$

to give

$$(v_\alpha)_{mn}{}^2=-\omega_{mn}{}^2(x_\alpha)_{mn}{}^2,$$

it is noted that for our case $(v_\alpha)_{mm}=0$ and, due to the fact that the wave functions are related to harmonic oscillator wave functions it is easily shown that for n different than $m\pm1$ the matrix elements are zero. Including all of these comments it is easy to prove that

(A18) may be written in the form

$$\mathcal{P}=ne^2\tau(E^0)^2\int_0^\infty dP_H\sum_{m=0}^{\infty}\sum_{\rho,\sigma}\omega_{m+1,\sigma;m,\rho}\times(\rho_{m,\rho}{}^{(0)}-\rho_{m+1,\sigma}{}^{(0)})(y_{m,\rho;m+1,\sigma})^2\times\left(\frac{1}{1+\tau^2(\omega+\omega_{m+1,\sigma;m,\rho})^2}+\frac{1}{1+\tau^2(\omega-\omega_{m+1,\sigma;m,\rho})^2}\right). \quad \text{(A19)}$$

The density matrix $\rho_{m,\rho}{}^{(0)}$ must now be written as

$$\rho_{m,\rho}{}^{(0)}=\exp\left[-\frac{\beta eH\hbar}{mc}E_{m,\rho}{}^{(0)}\right]\Big/\left\{2\int_0^\infty dP_H\sum_{n=0}^{\infty}\sum_{\sigma}\exp\left[-\frac{\beta eH\hbar}{mc}E_{n,\sigma}{}^{(0)}\right]\right\}. \quad \text{(A20)}$$

The subscripts ρ and σ refer to the eigenvalues attached to each quantum state n. The absorption line shape for a single transition, say from m,ρ to $m+1,\sigma$ will be denoted by $\mathcal{P}_{m,\rho;\sigma}$ and, neglecting the coefficient, may be written as

$$\mathcal{P}_{m,\rho;\sigma}=\int_0^\infty dP_H\,\omega_{m+1,\sigma;m\rho}(y_{m,\rho;m+1,\sigma})^2\times\left[\exp\left(-\frac{\beta eH\hbar}{mc}E_{m,\rho}{}^{(0)}\right)-\exp\left(-\frac{\beta eH\hbar}{mc}E_{m+1,\sigma}{}^{(0)}\right)\right]\times\left(\frac{1}{1+\tau^2(\omega+\omega_{m+1,\sigma;m,\rho})^2}+\frac{1}{1+\tau^2(\omega-\omega_{m+1,\sigma;m\rho})^2}\right)\times\left[1\Big/\int_0^\infty dP_H\sum_{n=0}^{\infty}\sum_{\nu}\exp\left(-\frac{\beta eH\hbar}{mc}E_{n,\nu}{}^{(0)}\right)\right]. \quad \text{(A21)}$$

The line-shape curve for $P_H=0$ is just the integrand taken at $P_H=0$.

PHYSICAL REVIEW VOLUME 122, NUMBER 2 APRIL 15, 1961

Reflection of Slow Electrons from Tungsten Single Crystals, Clean and with Adsorbed Monolayers

P. KISLIUK
Bell Telephone Laboratories, Murray Hill, New Jersey
(Received December 15, 1960)

The reflection of electrons with kinetic energy up to a few electron volts from tungsten single-crystal surfaces is measured both on the clean surface and with adsorbed monolayers of nitrogen and oxygen. For the clean surface, diffraction from the lattice is responsible for a considerable part of the reflection in the thermionic range of energy. The magnitude of the reflection is such as to have a barely measurable effect on experimental tests of the thermionic emission equations. This technique permits continuous recording of the change in work function as gas is adsorbed, yielding information about the kinetics of chemisorption and the surface dipoles due to the adsorbed gas atoms.

INTRODUCTION

THE well-known theoretical expression for the current density of thermionic electrons is[1,2]

$$J=A(1-\bar{R})T^2\exp(-\varphi/kT), \quad (1)$$

where A is 120 amp/cm^2 deg^2, $\bar{R}$ is the reflection coefficient averaged over the energy distribution, and φ is the work function. If the assumptions leading to this equation are valid, the energy distribution is Maxwellian except for the factor R, which may depend on the energy. MacColl[1,3] calculated R using a one-dimensional model with a sinusoidal internal potential connecting smoothly with an image potential at the barrier. He found about 5% reflection at zero kinetic energy of approach, falling rapidly at higher energy, with regions of 100% reflection very close to the energies where diffraction maxima are to be expected from the periodicity of the internal potential. The width of the region of 100% reflection in his examples is approximately equal to the amplitude of the sinusoidal internal variation in potential energy. It is, in fact, generally true in the weak-binding approximation that the width of the forbidden region is approximately equal to the matrix element of the periodic potential.[4]

For a more realistic model, one would expect to observe diffraction due to the three-dimensional space lattice. The effective mass, which enters into the calcu-

[1] C. Herring and M. H. Nichols, Revs. Modern Phys. 21, 185 (1949).
[2] W. B. Nottingham, *Handbuch der Physik*, edited by S. Flügge (Springer-Verlag, Berlin, 1956), Vol. 21, p. 1.
[3] L. A. MacColl, Bell System Tech. J. 30, 588 (1951).
[4] P. A. Wolff (private communication).